Possible candidate for the realization of the floating phase in the $S = \frac{5}{2}$ frustrated spin-chain model: $K_3Fe(MoO_4)_2(Mo_2O_7)$

K. Boya,[1,2] K. Nam,[3] K. Kargeti,[4] S. Ershadrad,[5] R. Kumar,[6] S. K. Panda,[4] B. Sanyal,[5] A. K. Manna,[7] P. L. Paulose,[6] Kee Hoon Kim,[3,*] and B. Koteswararao[1,†]

[1]*Department of Physics, Indian Institute of Technology Tirupati, Tirupati 517 619, India*
[2]*Government Polytechnic, Satyavedu, Andhra Pradesh 517 588, India*
[3]*Department of Physics and Astronomy and Institute of Applied Physics, Seoul National University, Seoul 151-747, Republic of Korea*
[4]*Department of Physics, Bennett University, Greater Noida, Uttar Pradesh 201310, India*
[5]*Department of Physics and Astronomy, Uppsala University, Box-516x, 75120 Uppsala, Sweden*
[6]*Department of Condensed Matter Physics and Materials Science, Tata Institute of Fundamental Research, Mumbai 400005, India*
[7]*Department of Chemistry, Indian Institute of Technology Tirupati, Tirupati 517 619, India*

(Received 24 December 2023; revised 30 January 2024; accepted 26 March 2024; published 10 April 2024)

The frustrated spin-chain (FSC) systems exhibit exotic ground states and distinct quantum phase transitions. The $S = \frac{1}{2}$ FSC is known to exhibit the Kosterlitz-Thouless transition from a commensurate gapless phase to a fully dimerized gapped phase upon the ratio of next-nearest-neighbor to nearest-neighbor coupling ($\alpha = \frac{J_2}{J_1}$) being tuned. On the other hand, the $S = \frac{5}{2}$ FSC system is known to show transitions from a commensurate gapless phase to partially dimerized and incommensurate floating phases [Chepiga, Affleck, and Mila, Phys. Rev. B **105**, 174402 (2022)]. While a large region of the floating phase has been theoretically predicted for the $S = \frac{5}{2}$ FSC model when $\alpha > 0.43$, it is yet to be explored experimentally. Here, we have investigated a compound $K_3Fe(MoO_4)_2(Mo_2O_7)$, having well-separated $S = \frac{5}{2}$ FSCs. The electronic structure calculations show that the $\alpha = \frac{J_2}{J_1}$ is close to 0.9, being similar to another FSC compound $Bi_3FeMo_2O_{12}$ ($\alpha \approx 1.1$). No magnetic long-range order is found down to 0.09 K, despite the relatively sizable Curie-Weiss temperature $\theta_{CW} = -18$ K. The magnetic heat capacity shows the power-law behavior, indicating that the compound exhibits gapless excitations. Based on the experimental results and the theoretical calculations employed by density functional theory, we argue that the titled system is a possible candidate for exhibiting the floating phase.

DOI: 10.1103/PhysRevB.109.155130

I. INTRODUCTION

The physics of low-dimensional and frustrated quantum magnets has attracted considerable attention to theoretical and experimental fronts in condensed-matter physics due to the realizations of novel states of matter [1–5]. The $S = \frac{1}{2}$ uniform Heisenberg antiferromagnetic (HAFM) spin-chain system holds the quasi-long-range ordering (LRO) as a ground state with gapless quasiparticle excitations [6], while the $S = 1$ spin chains hold the singlet ground state with gapped excitations [7,8]. The studies on frustrated spin chains (FSCs) with the competition between the first-nearest-neighbor (NN) coupling (J_1) and the second-NN coupling (J_2) are an excellent platform for exploring exotic quantum phase transitions (QPTs). The Hamiltonian describes the HAFM FSC models as follows:

$$H_{J_1-J_2} = -\sum_i (J_1 \mathbf{S}_i \cdot \mathbf{S}_{i+1} + J_2 \mathbf{S}_i \cdot \mathbf{S}_{i+2}). \quad (1)$$

In the case of the $S = \frac{1}{2}$ FSC or Majumdar-Ghosh (MG) spin-chain model [9], it undergoes a QPT of the Kosterlitz-Thouless type [10] from a gapless critical phase to a spontaneously dimerized phase with the opening of a spin gap when the value of $\alpha = \frac{J_2}{J_1}$ is greater than 0.241 [9,11–15]. When $\alpha = 0.5$, the model was exactly solved [9]. Recent theoretical studies on FSC models for various spin values provide diverse quantum phase diagrams with a wide variety of QPTs [16–19].

In the case of the $S = \frac{5}{2}$ FSC, the theoretical studies predict a remarkable sequence of several QPTs as a function of α. Those quantum phases are (i) a critical-commensurate phase for small values of α less than 0.3, (ii) a narrow region of partially dimerized and gapped phase for $\alpha \approx 0.3$ to 0.43, (iii) a broad region of floating phase when α is greater than 0.43, and (iv) finally, a fully dimerized phase for large values of α greater than 6 [19]. Here, the floating phase is a critical phase in which the spins are incommensurately correlated. It is a state with a quasi-LRO state exhibiting gapless excitations. The name "floating" arises from the fact that the wave vector of the dominant spin-spin correlation is not frozen, and it changes its state continuously with respect to α. According to the theoretical studies, the floating phase can be realized in $S = \frac{3}{2}$ and $S = \frac{5}{2}$ FSC systems. However, $S = \frac{5}{2}$ FSC can form a more broad region of the floating phase than the $S = \frac{3}{2}$ spin system [18,19]. To explore the possibility of experimental realization of the floating phase, we have chosen to study the $S = \frac{5}{2}$ FSC material.

*khkim@phya.snu.ac.kr
†koteswararao@iittp.ac.in

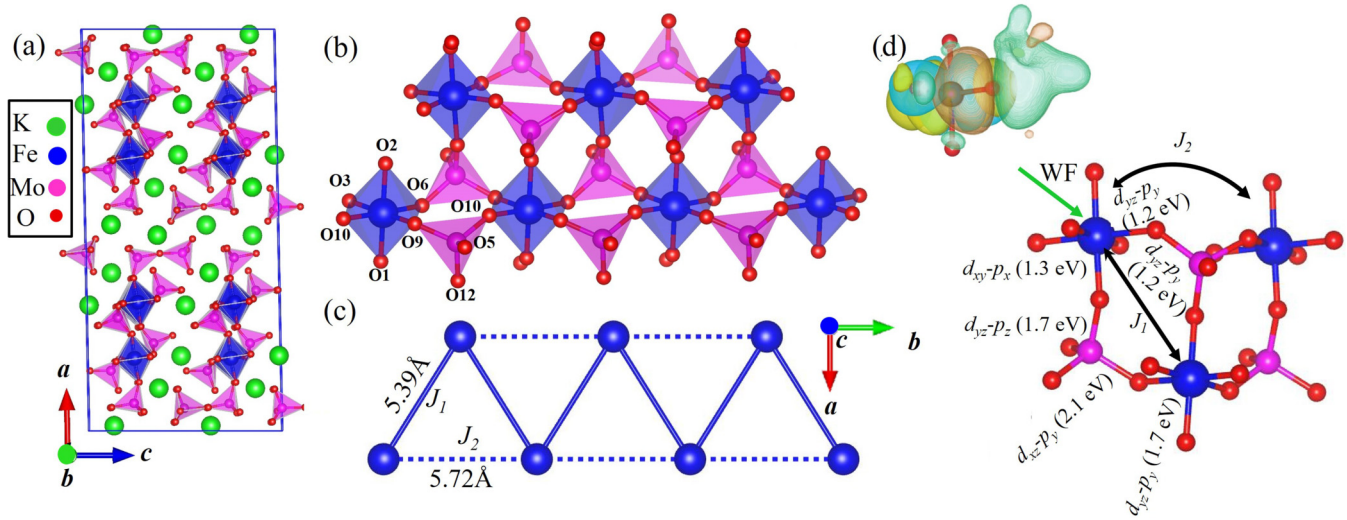

FIG. 1. (a) The unit cell of $K_3Fe(MoO_4)_2(Mo_2O_7)$. (b) The chains formed by the connected FeO_6 octahedral and MoO_4 tetrahedral units running along the b axis. (c) First NN (J_1) and second NN (J_2) of Fe-Fe bonds form the $S = \frac{5}{2}$ anisotropic triangular chains. (d) Illustration of the indirect exchange path, where the Mo and O atoms are active in the exchange. The values in parentheses are the strongest d-p orbital hopping parameters, dominant along the exchange path. The black arrows show the direct magnetic path of J_1 and J_2. The plot of maximally localized Wannier functions (MLWF) shows the sizable overlap between the d_{yz} orbital of Fe and the p_y orbital of O as an example of active orbitals along the exchange path (d_{yz} lobes are bright blue and yellow, and p_y lobes are bright green and orange).

A few examples of $S = \frac{5}{2}$ FSC systems include $Bi_2Fe(SeO_3)_2OCl_3$ [20] and $Bi_3FeMo_2O_{12}$ (BFMO) [21]. The compound $Bi_2Fe(SeO_3)_2OCl_3$ has zig-zag chains with $\alpha = 0.2$. However, the magnetic data show a broad maximum at about 130 K while it undergoes magnetic LRO at 13 K due to interchain interactions. The BFMO system shows the anisotropic triangular chains with $\alpha \approx 1.1$ and no LRO down to 0.2 K. Interestingly, the heat capacity [$C_p(T)$] data show the power-law behavior at low temperatures, indicating the gapless excitations. Due to the significant frustration ($f = 200$) and negligible interchain interactions, the BFMO system maintains a gapless spin-disordered ground state. To explore various phases mentioned in the phase diagram of $S = \frac{5}{2}$ FSC systems, one needs to look for ideal materials with negligible interchain interactions and strong magnetic frustration.

Herein, we have investigated the physical properties of an $S = \frac{5}{2}$ anisotropic triangular chain system $K_3Fe(MoO_4)_2(Mo_2O_7)$ (KFMO) by means of magnetic susceptibility $\chi(T)$, heat capacity measurements, and density functional theory (DFT) calculations. The $\chi(T)$ data show a broad maximum at 5 K, indicating the presence of short-range correlations. There is no splitting in the zero-field-cooling and field-cooling $\chi(T)$ data, indicating the absence of the spin freezing and/or spin-glass phase. The Curie-Weiss temperature is about -18 K, suggesting the presence of antiferromagnetic (AFM) interactions in the system. The magnetic heat capacity [$C_m(T)$] data show a broad maximum at 2.7 K and no sharp anomaly down to 0.09 K. The $C_m(T)$ data are consistent with power-law behavior at low temperatures and do not reach zero down to 0.09 K, indicating the presence of gapless excitations. The electronic structure calculations by DFT predict that the extracted exchange interactions are in the AFM nature. This AFM exchange interaction is indirect, mediated by oxygen and molybdenum atoms, as confirmed by the Wannier diagram. The value of α is found to be about 0.9. According to the predicted phase diagram of the HAFM model on FSCs with $S = \frac{5}{2}$ moments, the system with $\alpha \approx 0.9$ falls into the floating phase region.

II. METHODS

Polycrystalline samples of the compound KFMO were prepared using the solid-state synthesis method. The starting ingredients of high-purity chemicals, namely, K_2CO_3, MoO_3, and Fe_2O_3, were ground in a stoichiometric ratio and then fired at temperatures from 200 to 550 °C with multiple intermediate grindings. The single phase of the polycrystalline sample was confirmed using x-ray diffraction (XRD) at room temperature [22]. The magnetization and heat capacity experiments were performed on the polycrystalline pellets using the physical property measurement system (PPMS) and CF-150 dilution fridge (DF) (Leiden cryogenics) for varying the temperature and magnetic fields. Using the PPMS, the measurements were taken down to 1.8 K and up to the magnetic fields of 160 kOe. In addition, the low-temperature $C_P(T)$ measurements were carried out down to 0.09 K in both zero and applied magnetic fields. The DFT calculations were performed using the generalized gradient approximation (GGA) + Hubbard U in the VASP software.

III. RESULTS AND ANALYSIS

A. Structural aspects of $K_3Fe(MoO_4)_2(Mo_2O_7)$

The compound $K_3Fe(MoO_4)_2(Mo_2O_7)$ crystallizes in a monoclinic structure with space group $C2/c$ (No. 15) with large lattice constants: $a = 32.88$ Å, $b = 5.72$ Å, $c = 15.85$ Å, and $\alpha = \gamma = 90°$ and $\beta = 91.11°$ [22]. The Rietveld refinement on the powder XRD using the FULLPROF SUITE program confirms the single phase of the sample. The refinement parameters are $\chi^2 = 4.94$, $R_p = 16.7\%$, and $R_{wp} = 17.7\%$

TABLE I. The magnetic spin interactions with the exchange path and exchange energies of the $S = \frac{5}{2}$ FSC compound KFMO. The relative magnetic exchange energies are estimated from theoretical DFT calculations.

Interaction	Bond distance (Å)	Exchange path	Exchange energy (meV)	Ratio
J_1	5.39 Å	Fe-O-Mo-O-Fe	−2.22	1
J_2	5.72	Fe-O-Mo-O-Fe	−2.04	0.91

[23]. The unit cell has four formula units ($z = 4$). A single Fe atom is present in this formula unit, and it holds a Fe^{3+} oxidation state, leading to the magnetically active element with $S = \frac{5}{2}$ moments. The Fe^{3+} is in the distorted octahedral O^{2-} coordination. The unit cell contains FeO_6 octahedral, which is connected through MoO_4 polyhedral [see Fig. 1(b)]. The first-NN coupling between Fe-Fe distance is 5.39 Å. The zig-zag chains form by adding the second NN with Fe-Fe distance = 5.72 Å (see Fig. 1). The chains are running along the b direction. The possible exchange paths for the first NN and second NN (see Table I). The large interchain separations of 7.92 Å along the c direction and 11.88 Å along the a direction suggest that interchain magnetic interactions are weak and negligible.

B. Magnetization measurements

As shown in Fig. 2, temperature-dependent $\chi(T)$ measurements were carried out on the polycrystalline samples of KFMO down to 1.9 K in a 10-kOe field. The $\chi(T)$ data show no sharp anomaly, implying the absence of magnetic LRO in this system. They rather show a broad maximum at a temperature ($T^{\max}$) of about 5 K, suggesting the presence of short-range correlations stemming from the one-dimensional nature of the system [24,25]. The maximum value of magnetic susceptibility ($\chi^{\max}$) at $T^{\max}$ is about 0.16 cm^3/mol. The value of $\chi^{\max}T^{\max}/g^2 = 0.2$, which is much smaller than the expected value of 0.38 for the $S = \frac{5}{2}$ HAFM uniform spin-chain model [26,27]. A similar feature is also noticed in other $S = \frac{5}{2}$ HAFM FSC materials such as $Bi_2Fe(SeO_3)_2OCl_3$ ($\chi^{\max}T^{\max}/g^2 = 0.26$) [20] and $Bi_3FeMo_2O_{12}$ ($\chi^{\max}T^{\max}/g^2 = 0.17$) [21]. The reduction of the value compared to the $S = \frac{5}{2}$ HAFM uniform spin-chain model indicates the robustness of strong magnetic frustration. From our experimental observation of the $T^{\max}$ position, the J/k_B value is expected to be about −0.5 K [26,27].

The inverse-$\chi(T)$ data fit with the Curie-Weiss law ($\chi = \chi_0 + \frac{C}{T-\theta_{CW}}$) at high temperatures. The yielded $\theta_{CW} = -18$ K suggests that the dominant couplings are AFM. The effective magnetic moment is estimated from the Curie constant $C = \frac{N_A g^2 \mu^2 S(S+1)}{3k_B}$, where N_A is the Avogadro number and k_B is the Boltzmann constant. The yielded $\mu_{\text{eff}} =$

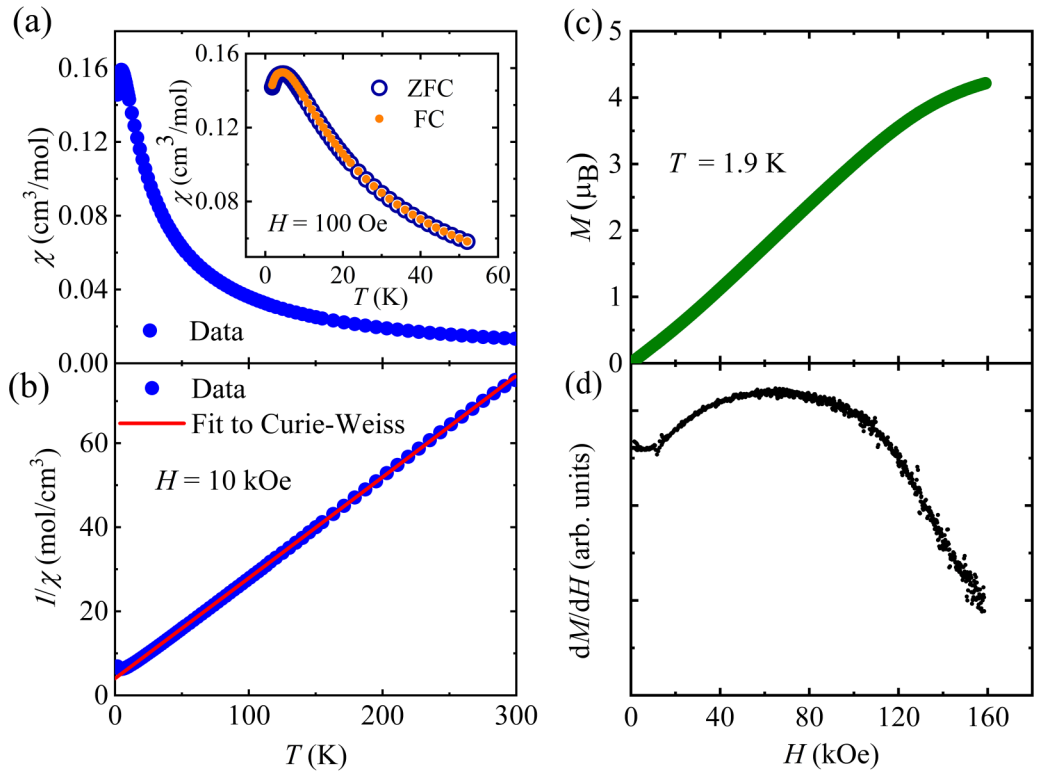

FIG. 2. (a) Temperature-dependent magnetic susceptibility $\chi(T)$ in the 10-kOe field. The inset of panel (a) shows the zero-field-cooled (ZFC) and field-cooled (FC) $\chi(T)$ data. (b) Inverse $\chi(T)$ data with Curie-Weiss fit. (c) Magnetic isotherm at 1.9 K up to 160 kOe. (d) Differential magnetization with respect to the magnetic field (dM/dH) as a function of H.

5.80 μ_B from the fit confirms the presence of $S = \frac{5}{2}$ moments and a Landé g factor of $g = 1.99$. The T-independent susceptibility (χ_0) is -1.09×10^{-4} cm^3/mol, due to the diamagnetism and Van Vleck paramagnetism [27]. The individual Pascal diamagnetic constants in the chemical formula are $K^+ = -14.9 \times 10^{-6}$ cm^3/mol, $Fe^{3+} = -10 \times 10^{-6}$ cm^3/mol, $Mo^{6+} = -7 \times 10^{-6}$ cm^3/mol, and $O^{2-} = -12 \times 10^{-6}$ cm^3/mol, and the calculated diamagnetic susceptibility χ_{dia} turns out to be -2.58×10^{-4} cm^3 per mol [28]. The extracted Van Vleck susceptibility is $\chi_{VV} = 1.49 \times 10^{-4}$ cm^3/mol Fe. There is no difference in zero-field-cooling (ZFC) and field-cooling (FC) magnetic data, ruling out the glassy behavior (see the inset of Fig. 2). Magnetization $M(H)$ was also measured at 1.9 K up to 160 kOe. The absence of hysteresis suggests that there are no ferromagnetic moments in the compound. As shown in Fig. 2, the $M(H)$ is linear at low fields. The deviation from the linearity is seen at high fields. The M value at 160 kOe is about 4 μ_B, so a higher magnetic field is required to get the saturated magnetic moment of 5 μ_B. To understand the ground-state properties of the system, one needs to look at thermodynamic properties at further low temperatures.

C. Heat capacity

The $C_p(T)$ measurement was carried out on the polycrystalline pellet of KFMO down to 0.09 K using a CF-150 DF (Leiden cryogenics) in the zero magnetic field (see Fig. 3). Interestingly, it does not show any anomaly in the $C_p(T)$ data, implying that no magnetic LRO is observed down to 0.09 K. The frustration parameter f ($=\frac{\theta_{CW}}{T_N}$) is greater than 200, indicating that the compound KFMO is a highly frustrated magnetic system. As the KFMO is an insulator, the $C_p(T)$ data do not have any itinerant electronic contribution. To extract the magnetic part of the $C_p(T)$, we used the Debye and Einstein model for estimating the lattice contribution. The Debye and Einstein model for the lattice heat capacity can be calculated by using the following equation [29]:

$$C(T) = 9R\sum_n d_n\left(\frac{T}{\theta_{Dn}}\right)^3 \int_0^{\frac{\theta_{Dn}}{T}} \frac{x^4 e^x}{(e^x-1)^2}dx + 3R\sum_n e_n\left(\frac{\theta_E}{T}\right)^2 \int_0^{\frac{T}{\theta_E}} \frac{e^{\frac{\theta_E}{T}}}{(e^{\frac{\theta_E}{T}}-1)^2}dT, \quad (2)$$

where $x = \frac{\theta_D}{T}$ and $\theta_E = \frac{h\nu}{k_B}$

Here, θ_D is the Debye temperature, θ_E is the Einstein temperature, d_n and e_n represent the coefficients, and R is the universal gas constant. The obtained Debye temperatures are $\theta_{D1} = 382$ K, $\theta_{E1} = 104$ K, and $\theta_{E2} = 651$ K. The extracted magnetic heat capacity $C_m(T)$ data show a broad maximum at 2.7 K, suggesting that it is due to the low-dimensional nature of the material; it has been observed in $\chi(T)$ data also. The magnetic entropy is estimated from the integration of $\frac{C_m}{T}$ data with respect to T, as shown in Fig. 3. This is in good agreement with the calculated entropy (14.87 J/mol K) for the $S = \frac{5}{2}$ system. The total entropy released below the Curie-Weiss temperature is a typical signature of frustrated magnetism. The $C_m(T)$ data are fitted with the power law $C_m \propto T^\beta$. The obtained exponent $\beta = 1.66$. The observation

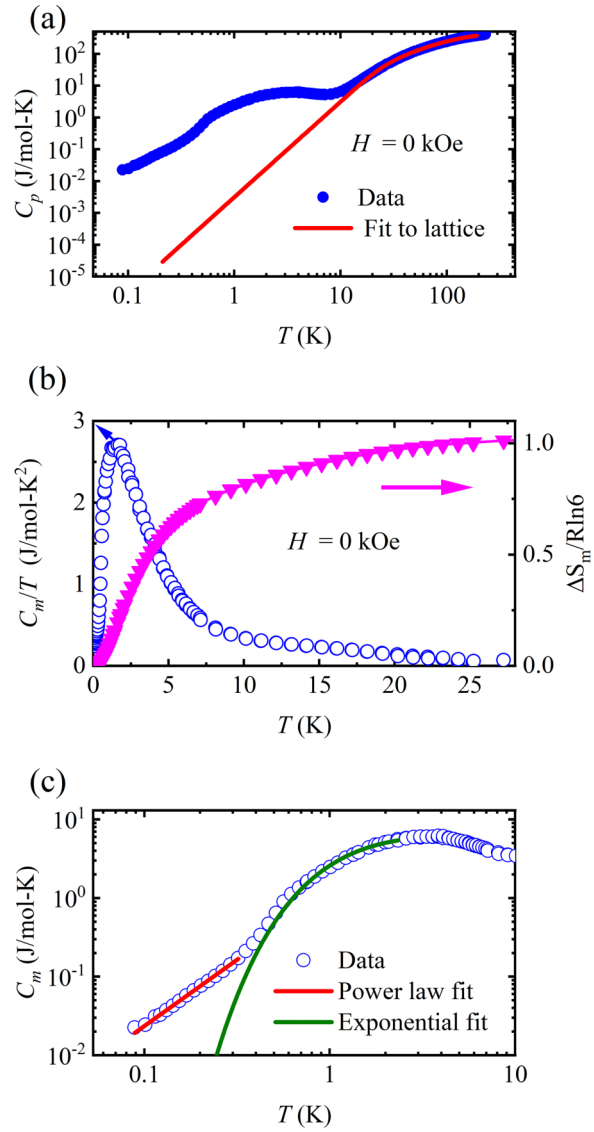

FIG. 3. (a) C_p versus T measured under zero field from 0.09 to 300 K. (b) $\frac{C_m}{T}$ versus T on the left y axis and normalized entropy versus T on the right y axis. (c) C_m versus T fitted with the power-law and exponential curves.

of power-law behavior at low temperatures indicates gapless excitations in the ground state. In addition, we have also compared the data with the fit to the exponential expression. The fact that the $C_m(T)$ data do not follow the exponential behavior confirms the absence of a spin gap in the ground state. Based on the C_m data analysis, it can be inferred that the KFMO system exhibits a gapless ground state.

D. Density functional theory calculations

To understand the ground-state electronic structure properties, we have performed *ab initio* DFT calculations within the GGA + Hubbard U approach using the simulation package RSPT [30]. Brillouin zone integration in k-space uses thermal smearing with $6 \times 3 \times 6$ mesh dimensions. The on-site Coulomb interaction (U) and the exchange term (J) for Fe-3d orbitals are considered to be 4.0 and 0.8 eV, respectively

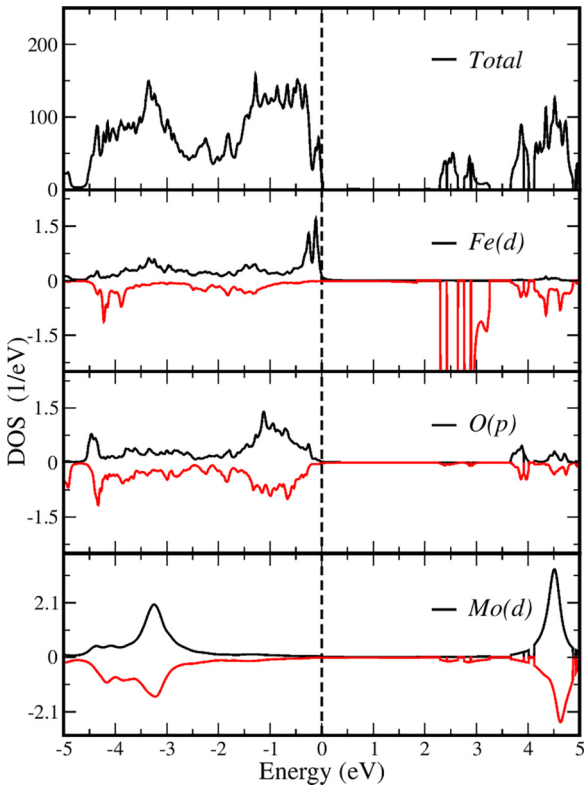

FIG. 4. The total and orbital-decomposed density of states (DOS) for the lowest energy magnetic state were obtained using GGA + U with $U = 4$ eV.

[31]. The partial and total density of states (DOS) have been obtained using the plane-wave-based method as implemented in the Vienna Ab initio Simulation Package (VASP) [32,33]. Figure 4 represents the total and partial DOS of the constituent atoms. The total DOS clearly exhibits the insulating ground states with a band gap of 2.29 eV. To understand the insulating nature of the system, the projected DOS for Fe-3d and O-2p states are also plotted. Since Fe-3d orbitals are half filled, we can observe that the majority channel (spin up) is completely occupied, lying below the Fermi energy, while the minority channel (spin down) is totally empty, located above the Fermi energy. The magnetic moment on the Fe site is 4.23 μ_B. Hence, the insulating nature of the system can be attributed to the local moment formation and the correlation effect of the Fe-3d orbital. The effective intersite exchange parameters (J_{ij}) were extracted from converged GGA + U calculations using the magnetic force theorem implemented in the RSPT code. The extracted exchange interactions are antiferromagnetic in nature, and the α value is nearly equal to 1, suggesting that the KFMO compound is an anisotropic triangular system, as shown in Table I. The magnetic exchange path follows a superexchange mechanism through Fe-O-Mo-O-Fe, as shown in Table I. The theoretical estimation of interchain interaction J can be found in Ref. [34], as shown in the following equation:

$$\exp\left(\frac{2|J|}{k_B T_N}\right) = \frac{4 + z\eta}{z\eta}, \tag{3}$$

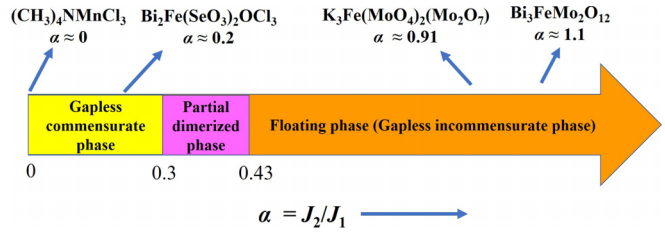

FIG. 5. Phase diagram of the $S = \frac{5}{2}$ frustrated chain with respect to $\alpha = \frac{J_2}{J_1}$ values [19]. The fully dimerized phase emerges for large values of α greater than 6.

where $\eta = \frac{J'}{J}$ is the ratio of interchain to intrachain interaction, and z is the number of nearest neighbors ($z = 4$). The $|J|/k_B$ value is about 0.5 K, extracted from the $T^{\max}$ position [27]. T_N is the Neel temperature. Since there is no T_N for the KFMO system, down to 0.09 K, we considered the value of the lowest measured temperature in place of T_N for extracting the minimum value of $\frac{J'}{J}$. Since the extracted $\frac{J'}{J}$ value is smaller than 0.01, the KFMO system is suggested to be a well-isolated triangular chain.

IV. DISCUSSION AND SUMMARY

Low-dimensional quantum spin systems appear to be simple but exhibit interesting quantum phases of condensed matter such as quantum spin liquid (QSL), valence bond solid (VBS), and a few more novel phases [35]. The past few decades have seen thorough investigations on the $S = \frac{1}{2}$ AFM FSC model theoretically. It is fully dimerized when the α value is greater than 0.24. The scenario is different for the FSCs with large spin values. For instance, the spin $S = 1$ chain system exhibits a clear spin gap over the whole range of α values, as per the Affleck-Kennedy-Lieb-Tasaki (AKLT) model [36]. The recent studies on $S = \frac{3}{2}$ and $\frac{5}{2}$ FSCs predicted the new phase of matter called the floating phase [18,19], which holds incommensurate short-range correlations. According to the $S = \frac{5}{2}$ FSC phase diagram (see Fig. 5), it exhibits various ground states with different values of α. The floating zone region starts with $\alpha = 0.43$ and ends at $\alpha = 6$, implying that it occupies a large region. This floating phase is sandwiched between the two spin-gapped regions of partially and fully dimerized phases.

A collection of the experimental candidates in the $S = \frac{5}{2}$ spin chains are mentioned in Table II. The nonfrustrated spin-chain system is $(CH_3)_4NMnCl_3$-TMMC having $\alpha = 0$, exhibiting the AFM ordering at $T_N = 0.83$ K [37]. It shows commensurate gapless excitations above the AFM order, as expected for nonfrustrated half-integer spin chains. In the case of a weakly FSC system ($\frac{J_2}{J_1} = 0.2$), the $S = \frac{5}{2}$ FSC system $Bi_2Fe(SeO_3)_2OCl_3$ shows the LRO at 13 K, which is probably due to non-negligible interchain interactions [20]. In order to get the highly disordered ground state, one needs isolated spin-chain systems with significant magnetic frustration. In Table II, the two $S = \frac{5}{2}$ highly FSC systems are shown. Recently, the results of the $S = \frac{5}{2}$ FSC compound BFMO imply the value of α is 1.1 [21], and it was predicted to be a candidate for a floating phase system by the Chepiga, Affleck, and Mila group [19]. Similarly, the results of KFMO hold the value of α

TABLE II. The details of a few $S = \frac{5}{2}$ spin-chain materials.

Compound	α	θ_{CW} (K)	T^{max} in $\chi(T)$	$\frac{\chi^{max}T^{max}}{g^2}$	$T_N(K)$	β	Possible ground state
$(CH_3)_4NMnCl_3$(TMMC)	0	−90	70	0.34	0.84	∼1	LRO
$Bi_2Fe(SeO_3)_2OCl_3$	0.2	–	130	0.26	13	–	LRO
$K_3Fe(MoO_4)_2(Mo_2O_7)$	0.9	−18	5	0.2	No LRO down to 0.09 K	1.66	Floating phase
$Bi_3FeMo_2O_{12}$	1.1	−40	10	0.17	No LRO down to 0.2 K	1.25	Floating phase

is 0.9 and show gapless behavior, strongly implying the titled compound might be a candidate material to exhibit a floating phase in the class of $S = \frac{5}{2}$ FSC systems.

In summary, we have investigated the compound $K_3Fe(MoO_4)_2(Mo_2O_7)$ having the well-separated $S = \frac{5}{2}$ FSCs through magnetic susceptibility $\chi(T)$ and heat capacity $C_P(T)$ measurements followed by the DFT electronic structure calculations. The electronic structure calculations show that the α value of $K_3Fe(MoO_4)_2(Mo_2O_7)$ is close to 0.9. No magnetic LRO is noticed even at 0.09 K temperatures, despite the relatively large antiferromagnetic $\theta_{CW} = -18$ K. The T-dependent magnetic heat capacity follows the power-law behavior, indicating that the compound KFMO exhibits gapless excitations. According to the $S = \frac{5}{2}$ FSC theoretical model's quantum phase diagram (QPD) (see Fig. 5), the KFMO ($\alpha \approx 0.9$) system should be a possible candidate for a floating phase with gapless excitations, similar to that of BFMO ($\alpha \approx 1.1$). However, to understand the exact ground state with quasiparticle excitations and confirm the floating phase, one needs to explore other experiments employing local probe techniques, such as muon spin rotation and inelastic neutron scattering techniques.

ACKNOWLEDGMENTS

B.K. and S.K.P. acknowledge support from SERB (Grant No. CRG/2023/003063) from DST India. The work at SNU was supported by the NRF through the Quantum Computing Research Infrastructure Construction program (Grant No. 2022M3K2A1083855) and by the Ministry of Education through the Core Center program (Grant No. 2021R1A6C101B418). The computations were provided by resources provided by the Swedish National Infrastructure for Computing (SNIC) (Project No. SNIC 2021/3-38) at NSC, PDC, and HPC2N, partially funded by the VR (Grant No. 2018-05973). B.S. acknowledges allocation of supercomputing hours by the PRACE DECI-17 project "Q2Dtopomat" at the Eagle supercomputer in Poland and EuroHPC resources at the Karolina supercomputer in the Czech Republic. B.S. and S.E. acknowledge EuroHPC resources at Finland's LUMI supercomputer (Grants No. EHPC-DEV-2022D10-059 and No. EHPC-DEV-2022D10-057).

[1] A. Vasiliev, O. Volkova, E. Zvereva, and M. Markina, Milestones of low-D quantum magnetism, npj Quantum Mater. **3**, 18 (2018).

[2] C. Broholm, R. Cava, S. Kivelson, D. Nocera, M. Norman, and T. Senthil, Quantum spin liquids, Science **367**, eaay0668 (2020).

[3] L. Balents, Spin liquids in frustrated magnets, Nature (London) **464**, 199 (2010).

[4] L. Savary and L. Balents, Quantum spin liquids: a review, Rep. Prog. Phys. **80**, 016502 (2017).

[5] J. Wen, S.-L. Yu, S. Li, W. Yu, and J.-X. Li, Experimental identification of quantum spin liquids, npj Quantum Mater. **4**, 12 (2019).

[6] M. Mourigal, M. Enderle, A. Klöpperpieper, J.-S. Caux, A. Stunault, and H. M. Rønnow, Fractional spinon excitations in the quantum Heisenberg antiferromagnetic chain, Nat. Phys. **9**, 435 (2013).

[7] F. D. M. Haldane, Continuum dynamics of the 1-D Heisenberg antiferromagnet: Identification with the O(3) nonlinear sigma model, Phys. Lett. A **93**, 464 (1983).

[8] F. D. M. Haldane, Nonlinear field theory of large-spin Heisenberg antiferromagnets: Semiclassically quantized solitons of the one-dimensional easy-axis Néel state, Phys. Rev. Lett. **50**, 1153 (1983).

[9] C. K. Majumdar and D. K. Ghosh, On next-nearest-neighbor interaction in linear chain. I, J. Math. Phys. **10**, 1388 (1969).

[10] J. M. Kosterlitz and D. J. Thouless, Ordering, metastability and phase transitions in two-dimensional systems, J. Phys. C **6**, 1181 (1973).

[11] K. Okamoto and K. Nomura, Fluid-dimer critical point in $S = \frac{1}{2}$ antiferromagnetic Heisenberg chain with next nearest neighbor interactions, Phys. Lett. A **169**, 433 (1992).

[12] A. K. Kolezhuk, R. Roth, and U. Schollwöck, First order transition in the frustrated antiferromagnetic Heisenberg $S = 1$ quantum spin chain, Phys. Rev. Lett. **77**, 5142 (1996).

[13] A. K. Kolezhuk and U. Schollwöck, Connectivity transition in the frustrated $S = 1$ chain revisited, Phys. Rev. B **65**, 100401(R) (2002).

[14] S. Lebernegg, O. Janson, I. Rousochatzakis, S. Nishimoto, H. Rosner, and A. A. Tsirlin, Frustrated spin chain physics near the Majumdar-Ghosh point in szenicsite $Cu_3(MoO_4)(OH)_4$, Phys. Rev. B **95**, 035145 (2017).

[15] R. W. Chhajlany, P. Tomczak, A. Wójcik, and J. Richter, Entanglement in the Majumdar-Ghosh model, Phys. Rev. A **75**, 032340 (2007).

[16] S. R. White and I. Affleck, Dimerization and incommensurate spiral spin correlations in the zigzag spin chain: Analogies to the Kondo lattice, Phys. Rev. B **54**, 9862 (1996).

[17] R. Roth and U. Schollwöck, Frustrated antiferromagnetic quantum spin chains for spin length $S > 1$, Phys. Rev. B **58**, 9264 (1998).

[18] N. Chepiga, I. Affleck, and F. Mila, Floating, critical, and dimerized phases in a frustrated spin-$\frac{3}{2}$ chain, Phys. Rev. B **101**, 174407 (2020).

[19] N. Chepiga, I. Affleck, and F. Mila, From SU(2)5 to SU(2)3 Wess-Zumino-Witten transitions in a frustrated spin-$\frac{5}{2}$ chain, Phys. Rev. B **105**, 174402 (2022).

[20] P. S. Berdonosov, E. S. Kuznetsova, V. A. Dolgikh, A. V. Sobolev, I. A. Presniakov, A. V. Olenev, B. Rahaman, T. Saha-Dasgupta, K. V. Zakharov, E. A. Zvereva *et al.*, Crystal structure, physical properties, and electronic and magnetic structure of the spin $S = \frac{5}{2}$ zigzag chain compound $Bi_2Fe(SeO_3)_2OCl_3$, Inorg. Chem. **53**, 5830 (2014).

[21] K. Boya, K. Nam, A. K. Manna, J. Kang, C. Lyi, A. Jain, S. M. Yusuf, P. Khuntia, B. Sana, V. Kumar, A. V. Mahajan, D. R. Patil, K. H. Kim, S. K. Panda, and B. Koteswararao, Magnetic properties of the $S = \frac{5}{2}$ anisotropic triangular chain compound $Bi_3FeMo_2O_{12}$, Phys. Rev. B **104**, 184402 (2021).

[22] M. Maczka, A. Pietraszko, W. Paraguassu, A. Souza Filho, P. Freire, J. Mendes Filho, and J. Hanuza, Structural and vibrational properties of $K_3Fe(MoO_4)_2(Mo_2O_7)$—a novel layered molybdate, J. Phys.: Condens. Matter **21**, 095402 (2009).

[23] J. Rodríguez-Carvajal, Recent advances in magnetic structure determination by neutron powder diffraction, Physica B **192**, 55 (1993).

[24] B. Koteswararao, S. K. Panda, R. Kumar, K. Yoo, A. V. Mahajan, I. Dasgupta, B. Chen, K. H. Kim, and F. Chou, Observation of $S = \frac{1}{2}$ quasi-1D magnetic and magneto–dielectric behavior in a cubic $SrCuTe_2O_6$, J. Phys.: Condens. Matter **27**, 426001 (2015).

[25] R. Nath, A. V. Mahajan, N. Büttgen, C. Kegler, A. Loidl, and J. Bobroff, Study of one-dimensional nature of $S = \frac{1}{2}(Sr, Ba)_2Cu(PO_4)_2$ and $BaCuP_2O_7$ via P^{31} NMR, Phys. Rev. B **71**, 174436 (2005).

[26] Y. Kim, M. Greven, U.-J. Wiese, and R. Birgeneau, Monte-Carlo study of correlations in quantum spin chains at non-zero temperature, Eur. Phys. J. B **4**, 291 (1998).

[27] L. J. De Jongh and A. R. Miedema, Experiments on simple magnetic model systems, Adv. Phys. **50**, 947 (2001).

[28] G. A. Bain and J. F. Berry, Diamagnetic corrections and Pascal's constants, J. Chem. Educ. **85**, 532 (2008).

[29] C. Kittel, *Introduction to Solid State Physics* (Wiley & Sons, New York, 2004).

[30] J. M. Wills, O. Eriksson, M. Alouani, and D. L. Price, Full-potential LMTO total energy and force calculations, in *Electronic Structure and Physical Properties of Solids: The Uses of the LMTO Method Lectures of a Workshop Held at Mont Saint Odile, France, October 2–5, 1998* (Springer, Berlin, 2000), pp. 148–167.

[31] V. I. Anisimov, F. Aryasetiawan, and A. I. Lichtenstein, First-principles calculations of the electronic structure and spectra of strongly correlated systems: the LDA + U method, J. Phys.: Condens. Matter **9**, 767 (1997).

[32] G. Kresse and J. Hafner, *Ab initio* molecular dynamics for liquid metals, Phys. Rev. B **47**, 558 (1993).

[33] G. Kresse and J. Furthmüller, Efficient iterative schemes for *ab initio* total-energy calculations using a plane-wave basis set, Phys. Rev. B **54**, 11169 (1996).

[34] T. Oguchi, Exchange interactions in $Cu(NH_3)_4SO_4H_2O$, Phys. Rev. **133**, A1098 (1964).

[35] Y. Zhou, K. Kanoda, and T.-K. Ng, Quantum spin liquid states, Rev. Mod. Phys. **89**, 025003 (2017).

[36] I. Affleck, T. Kennedy, E. H. Lieb, and H. Tasaki, Valence bond ground states in isotropic quantum antiferromagnets, Commun. Math. Phys. **115**, 477 (1988).

[37] W. J. M. De Jonge, C. Swüste, K. Kopinga, and K. Takeda, Specific heat of nearly-one-dimensional tetramethyl ammonium manganese trichloride (TMMC) and tetramethyl ammonium cadmium trichloride (TMCC), Phys. Rev. B **12**, 5858 (1975).